Investigation of Ti Addition Effects on the Thickness of 55 pct Al-Zn-1.6 pct Si Coating by First-Principles Calculation

GUANGXIN WU, JIEYU ZHANG, YULING REN, GUOYANG LI, XIAOCHUN WU, QIAN LI, and KUOCHIH CHOU

First-principles method was performed to predict the effect of Ti addition on thickness and adhesion of 55 pct Al-Zn-1.6 pct Si coating. The results of optimized geometric configurations, total energy, and charge distributions for the Ti substitution in Fe2Al5 and FeAl3 phases indicated Ti will grab electronic charges from Al atoms, form bonds with neighboring Al, which will reduce the growth of Fe-Al intermetallic layers, and finally enhance the adhesion of the coating/substrate. Furthermore, experiments were performed to validate the prediction results of first-principles successfully.

DOI: 10.1007/s11661-011-1037-9

I. INTRODUCTION

THE application of a metallic coating by continuous hot-dip processing is one of the most widely used means of protecting steel against severe atmospheric corrosion. The 55 pct Al-Zn-1.6 pct Si coated steel product (GALVALUME, BIEC International Inc., Vancouver, WA) is one of the popular alloys in the building industries, and it has distinct advantages by providing not only better anticorrosive performance than that of zinc coating but also a high-temperature oxidation resistance the same as aluminum coating.[1] Therefore, these alloys have attracted extensive interest worldwide.

The presence of alloying elements in the bath was shown to affect strongly the morphology, kinetics, and growth of the zinc-aluminum coatings during the hot-dip process. Ti, RE, Mg, and Ni are the most common elements that are present either as deliberate alloying additions or as impurities originating from the raw materials used in the process. The addition of Ti to this known composition of 55 pct Al-Zn-Si coating was proposed in several patents and the literature for a number of years.[2–4] In Zn-11 pct Al-3 pct Mg-0.2 pct Si coating, it was shown that Ti-Al intermetallic phases are observed mainly in the centers of the refined Zn-Al alloy-coating layer, which suggests that $TiAl_3$ acts as a heterogeneous nucleation site of the primary Al phase.[5] Meanwhile, it is well known that the spangle size is determined by the nucleation and growth rates of the Al-rich primary dendritic network at the intermetallic layer interface.[6] Therefore, it would be expected that Ti additions to the liquid bath would enhance the nucleation rate when solidification takes place on the surface of the strip as it leaves the pot. This effect would cause then an additional refining effect on the spangle size of the strip and improve its surface properties.[7,8]

Because we know that the thickness of the intermetallic layer between iron substrate and coating is an important factor affecting the engineering quality of coated materials. The effect of the two alloy elements on the thickness of the intermetallic layer was interpreted as follows. The atom saturation in the Fe_2Al_5 phase is merely 70 pct, and the concentration of the vacant site in the *C*-axis direction is high, through which the Al atom easily diffuses into the boundary of Fe to form a new compound layer and grows rapidly in the *C*-axis direction. Because of alloy element addition, some atoms diffuse into the Fe_2Al_5 intermetallic layer and fill into the vacant site in the Fe_2Al_5 phase.[9] This behavior reduces the opportunity for the diffusion of Al atoms. As a result of the preceding reasons, the growth rate of the intermetallic layer was changed.[10] However, until recently, very little has been known about the underlying mechanism of Ti addition. Especially considering the little additive amounts, common equipment could not obtain the distribution of Ti inoculation. Therefore, first-principles is one of the extremely useful methods available to obtain the details from a micro view.

The purpose of the present study is to investigate the effect of Ti on the thickness of intermetallic layer and adhesion of coating/substrate with calculated bonding energy and charge transfer based on first-principles method.

II. METHODOLOGY

The calculations performed in this study were done using the Vienna *ab-initio* simulation package (VASP).[11] This program evaluates the total energy of periodically repeating geometries based on density-functional theory and the pseudo potential approximation. In this case, theelectron-ion interaction can be described by the projector augmented wave (PAW) method of Blöchl in

GUANGXIN WU, JIEYU ZHANG, XIAOCHUN WU, KUOCHIH CHOU, and QIAN LI, Professors, are with the School of Materials Science and Technology, Shanghai University, Shanghai 200072, P.R. China. Contact e-mail: gxwu@shu.edu.cn YULING REN and GUOYANG LI, Professors, are with the Cold Rolling Plant, Baosteel Branch, Baoshan Iron & Steel Co. Ltd., Shanghai 200941, P.R. China.

Manuscript submitted June 27, 2011.
Article published online February 11, 2012

the implementation of Kresse and Joubert.[12] The density of state is projected onto a sphere of radius 2.46, 2.50, and 2.50 Å for Fe ($3d^7$ $4s^1$core), Al ($2d^3$ $3s^1$ core), and Ti ($3d^3$ $4s^1$ core), respectively, to calculate the local electron distribution in all the supercells. The generalized gradient approximation (GGA) through the Perdew–Wang 91 (PW91)[13] functional was used for the exchange-correlation potential. Electron smearing is employed *via* the Methfessel–Paxton technique,[14] with a smearing width consistent with 0.1 eV, in order to minimize the errors in the Hellmann–Feynman forces due to the entropic contribution to the electronic free energy.[11] All energies are calculated at 0 K. The minimization of the electronic free energy is carried out using an efficient iterative matrix diagonalization routine based on a sequential band-by-band residuum minimization method[15] or, alternatively, based on preconditioned band-by-band conjugate gradient minimization.[16] The optimization of different atomic configurations is based upon a conjugate gradient minimization of the total energy. The values of the energy cutoffs and the *k*-point grids are chosen to ensure the convergence of energies and structures.

The electronic structures of Fe_2Al_5 and $FeAl_3$ were first studied by constructing ($2 \times 1 \times 2$) and ($2 \times 2 \times 2$) supercells consisting of 64 and 56 atoms (Figure 1). To simulate a RE substitution at the Fe or Al site, the Ce element was ignored due to the exiguous content. Therefore, the $(Fe,Ti)_2Al_5$, $Fe_2(Al,Ti)_5$, (Fe,Ti)Al3, and $Fe(Al,Ti)_3$ supercells were created. The corresponding kinetic energy cutoffs were 400 eV for all PAW calculations. Brillouin-zone integrations employed a $5 \times 5 \times 5$ Monkhorst–Pack grid of *k* points for all the calculation models.

The 55 pct Al-Zn-1.6 pct Si(-Ti) alloy samples for hot dip were taken from commercial products. The actual compositions of the steels and liquid bath detected by the chemical analysis method are given in Table I.

Light optical microscopy (LOM) of samples from each set of dipping conditions was used to characterize the morphologies of the cross section. The surface of the specimen was mechanically polished with 6- and 1-mm diamond pastes. After polishing, the sample was etched with 5 pct nitric acid alcohol for 5 seconds to reveal the microstructure of the overlay, and the microstructure of the interfacial layer was revealed by Keller's etch (2 mL HF, 3 mL HCL (conc.), 5 mL HNO_3 (conc.), and 190 mL water). Examination of the coating surface and internal microstructure was carried out using scanning electron microscopy (Apollo300 fitted with the INCA X-ray–EDS Germanium detector, Oxford Instruments, Abingdon, Oxfordshire).

III. RESULTS AND DISCUSSION

The accuracy of the computational method used in this study was tested initially to describe the properties of bulk Fe_2Al_5 and $FeAl_3$. In Table II, we provide the results for the equilibrium lattice constant and enthalpy of formation of Fe_2Al_5 and $FeAl_3$ together with corresponding experimental data and other previous calculations. Good agreement with experiment gives evidence of the accuracy of the GGA and the pseudo potentials used.

The data obtained in the previously presented tests indicate that there is good agreement of our calculated results for bulk Fe_2Al_5 and $FeAl_3$ with data obtained in other theoretical or experimental studies. These characteristics make us confident to pursue the next step of our investigations, namely, the effect of Ti addition on the thickness of the intermetallic layer in Al-Zn-Si hot-dip continuous coating.

The total energies of Ti substitution in structures are shown in Table III. It can be concluded that the energies of Ti substitution at Al sites in the Fe_2Al_5 and $FeAl_3$ are lower compared to the energies at Fe sites with a value of 5.5 eV. This means the most favorable sites for Ti substitution in both Fe_2Al_5 and $FeAl_3$ are Al positions. Therefore, in the calculation of the subsequent bonding energies and electronic structures, we mainly perform on $Fe_2(Al,Ti)_5$ and $Fe(Al,Ti)_3$ supercells.

Table I. Composition of Coating Baths

Bath	Al (Wt Pct)	Zn (Wt Pct)	Si (Wt Pct)	Fe (Wt Pct)	Ti (Wt Pct)
GL	55.57	42.63	2.33	0.15	<0.01
GL + Ti	51.00	36.15	1.61	0.11	<0.05

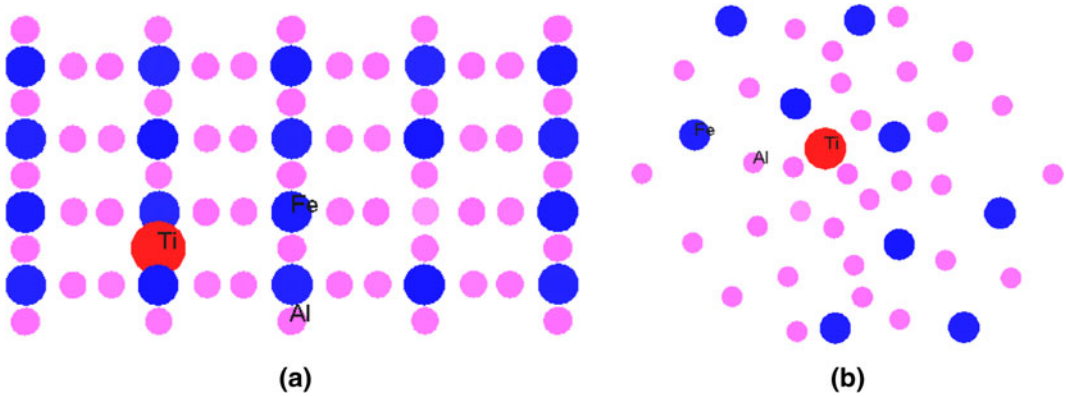

Fig. 1—Schematic representation of Ti substitution in (*a*) Fe_2Al_5 bulk and (*b*) $FeAl_3$ bulk. The larger, medium, and smaller spheres indicate Ti, Fe, and Al atoms, respectively.

Table II. Calculated Equilibrium Lattice Constant (a_0, b_0, c_0) and Enthalpy of Formation (ΔH) for Bulk Fe_2Al_5 and $FeAl_3$

Phase	Reference	a_0 (nm)	b_0 (nm)	c_0 (nm)	ΔH (kJ/mol)
Fe_2Al_5	this work	0.749	0.620	0.483	–176.6
	experiment	0.766*	0.639*	0.419*	–194.0**
$FeAl_3$	this work	1.542	0.804	1.244	–98.5
	experiment	1.549†	0.808†	1.247†	–112.6**

*Experimental value from Ref. 17.
**Experimental value from Ref. 18.
†Experimental value from Ref. 19.

Table III. Total Energy and Bonding Energy of Pure and Ti Substitution of Fe_2Al_5 and $FeAl_3$

	Total Energy (eV)		Bonding Energy (eV)	
Phase	Fe	Al	Fe-Al	Ti-Al
Fe_2Al_5	–324.134	–329.121	–0.824	–5.615
$FeAl_3$	–258.118	–264.648	–1.756	–7.120

The bonding energy ΔE between the Ti and Al is defined as follows:

$$\Delta E = E_{Fe_2(Al,Ti)_5} - E_{Ti} - E_{Fe_2(Al,void)_5} \quad [1]$$

and

$$\Delta E = E_{Fe(Al,Ti)_3} - E_{Ti} - E_{Fe(Al,void)_3} \quad [2]$$

where $E_{Fe_2(Al,Ti)_5}/E_{Fe_2(Al,Ti)_5}E_{Fe(Al,La)_3}E_{Fe(Al,La)_3}$ is the total energy of the $Fe_2(Al,Ti)_5/Fe(Al,Ti)_3$ system, $E_{Ti}$is the energy of the Ti atom, and $E_{Fe_2(Al,void)_5}/E_{Fe_2(Al,void)_5}E_{Fe(Al,void)_3}E_{Fe(Al,void)_3}$ is the total energy of the corresponding $Fe_2Al_5/FeAl_3$ structures in which one Al atom was removed. With this definition, negative values of bonding energy denote more stability than the corresponding void structure and atomic Ti.

The calculated bonding energies between Fe-Al and Ti-Al are also shown in Table III. The results show that the bonding energies between Ti and Al are obviously stronger than the bonding energy between Fe and Al. This means that the addition the Ti atom may effectively prevent Al from forming a metallic bond with iron and, therefore, inhibit Fe-Al growth.

Then, the charge transfers of Ti substitution are calculated (Figure 2), and the net charges of Al, Fe, and Ti are shown in Table IV. From Table IV and Figure 2, it is interesting to find that after Ti is added, the net electronic charges of Fe decrease about 0.013 and 0.026 for Fe_2Al_5 and $FeAl_3$, respectively. Meanwhile, the net electronic charges of Al almost do not change while the net charge of Ti is greatly higher. This finding indicates that the electronic charge of Al shifts to the Ti atom more significantly than to the Fe atom. As we know, electronic charge shift is an obvious bonding characteristic between effective additives and the matrix.[20,21] Therefore, it can be deduced that the addition Ti will grab electronic charges from Al atoms when they form the Ti-Al bond and reduce the coating thickness.

In this section, we will use the electronic density of states (DOS) to interpret the preceding results. The DOS was calculated as the average of a few hundred configurations distributed over the entire simulation. The calculated electronic DOS values for the four systems are presented in Figure 3. The origin of the energy is taken to be the Fermi level. The states can be classified as *s*, *p*, and *d* states. The identification of these features is made straightforward by the examination of the partial DOS on the states, which are also shown in Figure 3. We should emphasize that spin polarization is not included in our calculation, because magnetic moments of Fe_2Al_5 and $FeAl_3$ are zero, although the Fe atom has a strong paramagnetic character.[22]

For all four systems, it is found that the DOS of the intensity of Al states is very small from –2 eV up to the Fermi level. Therefore, the valence bands are dominated solely by the strong attractive potential of the Fe states. In this sense, the Fe-Al ensemble may be a charge-transfer compound. Furthermore, the strong resemblance of the DOS of the Fe-Al ensemble with the Fe DOS indicates that the DOS of Fe-Al is strongly dominated by Fe states. For the $Fe_2(Al,Ti)_5$ and $Fe(Al,Ti)_3$ systems, we note that at the Al site, states from bands at –1.8, –1.4 (Fe_2Al_5), and –2.2 ($FeAl_3$) eV have mixed *s*, *p*, *d* character, while the characters of the band close to Fermi level are both Al-*p*. At the Fe and Ti sites, the characters of the band close to Fermi level are Fe-*d* and Ti-*d*. This shows that the states mainly arise from the *d* bands. Meanwhile, in Figure 3, we see only very small changes in the Al and Fe DOS after Ti addition to the Fe_2Al_5 and $FeAl_3$. By contrast, the DOS for the Ti atom exhibits a large shift in its occupied states. This indicates that charge has been transferred to the Ti atom, which is consistent with the charge transfer seen in the electron density difference maps. Thus, all indicators point to the conclusion that the during the hot-dip process, strong adhesion of the GL/Fe interface is due to the bonds formed between Ti and neighboring Al, which will prevent the interaction between Fe and Al, reduce the growth of Fe-Al intermetallic layers, and finally enhance the adhesion. However, we caution that interpretation of these projections can only be trusted in a qualitative sense due to the numerical approximations employed and the somewhat arbitrary choice of cutoff radii.

The purpose of this section is to validate our calculation results. Image analysis was used to characterize the thicknesses of intermetallic layers for GL and GL + Ti baths. For the sake of measurement precision,

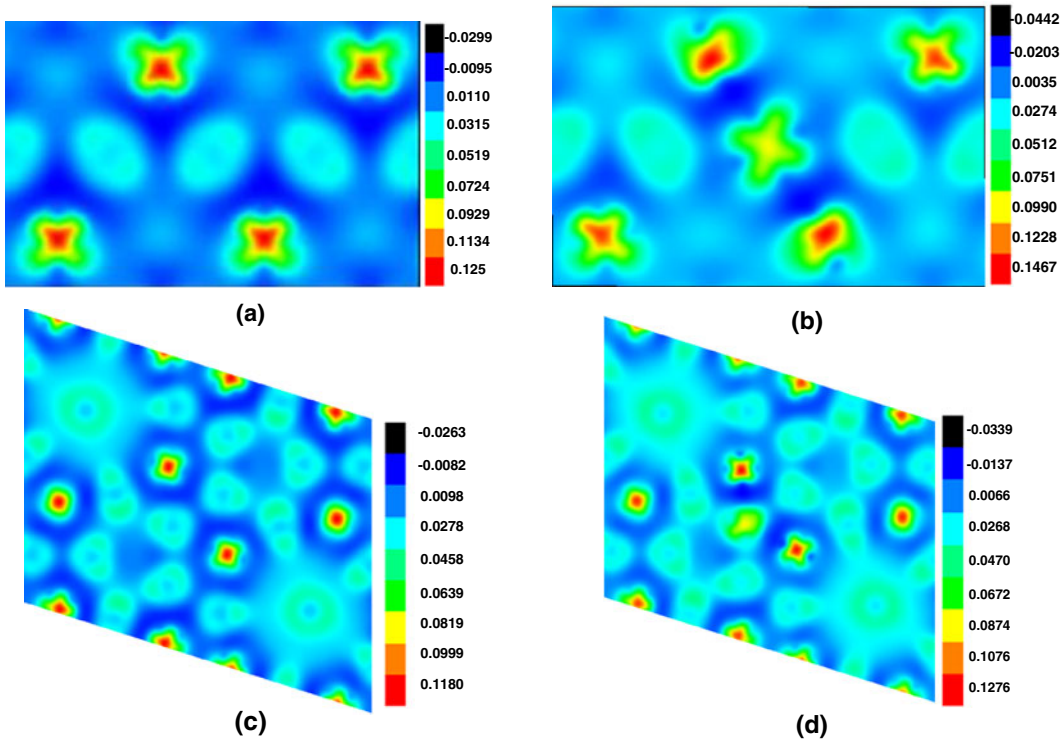

Fig. 2—(*a*) Charge transfer profile of pure, Ti substitution of (*b*) Fe_2Al_5 (400) and (*c*) pure, and (*d*) Ti substitution of $FeAl_3$ (110).

Table IV. Net Charge of Pure and Ti Substitution of Fe_2Al_5 and $FeAl_3$

	Net Charge		
Phase	Al	Fe	Ti
Fe_2Al_5			
pure	0.810	7.417	—
Ti-sub	0.811	7.405	3.449
$FeAl_3$			
pure	0.807	7.510	—
Ti-sub	0.807	7.504	3.314

five metallographic images of the reaction layer were captured for each sample and three measurement points were selected for each image. The total thickness of the intermetallic layer was calculated by averaging the testing values of 15 measurement points for each sample. These results are presented in Figures 4 and 5, with the error bars comprised of plus/minus one standard deviation across each sample group. The results were assessed statistically by applying a *t*-test analysis based on SAS 8.1, and results show that there is a statistically significant difference (statistical significance $P = 0.0016 < 0.05$) between the sample groups.

From Figure 4, it can be concluded that there is a rapid exothermic reaction between the Zn-Al-Si coating and the steel substrate by promoting the formation of a thin and continuous intermetallic alloy layer at the coating/steel interface. This solid reaction layer is comprised of Fe_2Al_5, $FeAl_3$, and $\alpha(\beta)$-FeAlSi phases[23,24] acting as a barrier preventing the reaction species, probably aluminum, from rapidly reaching the steel substrate. From Figure 5, it can be shown that Ti additions to the bath result in a significant decrease in the average thickness of the intermetallic layer. As can be seen, the average thickness decreased from 1.1 to 0.9 μm. We also note that our experiment result could be confirmed by García *et al.*,[7,8] which shows that the thickness of Ti causes an additional overall decrease of the alloyed layer thickness from 1.2 to 0.8 μm with Si content of 1.4 wt pct.

All preceding results indicate that our experimental result is consistent with the prediction result of the first-principles calculation. Furthermore, more uniform and thinner alloyed layers are expected to improve the performance of coated steel strips during sheet metal forming operations. The present results not only help to predict and clarify the experimentally observed Ti addition reducing the thickness of the intermetallic layer in the Al-Zn-Si coating, but may also help to design other types of hot-dip coating for practical applications in the building and auto industry.

IV. CONCLUSIONS

In conclusion, the first-principles method was used to investigate the effect of Ti addition on the thickness of the intermetallic layer in hot-dip Al-Zn coating. The optimized geometric configurations, total energy, and electronic charge distributions for the Ti substitution in Fe_2Al_5 and $FeAl_3$ phases were calculated. The results indicated that the most favorable sites for Ti substitution in both Fe_2Al_5 and $FeAl_3$ phases are Al positions.

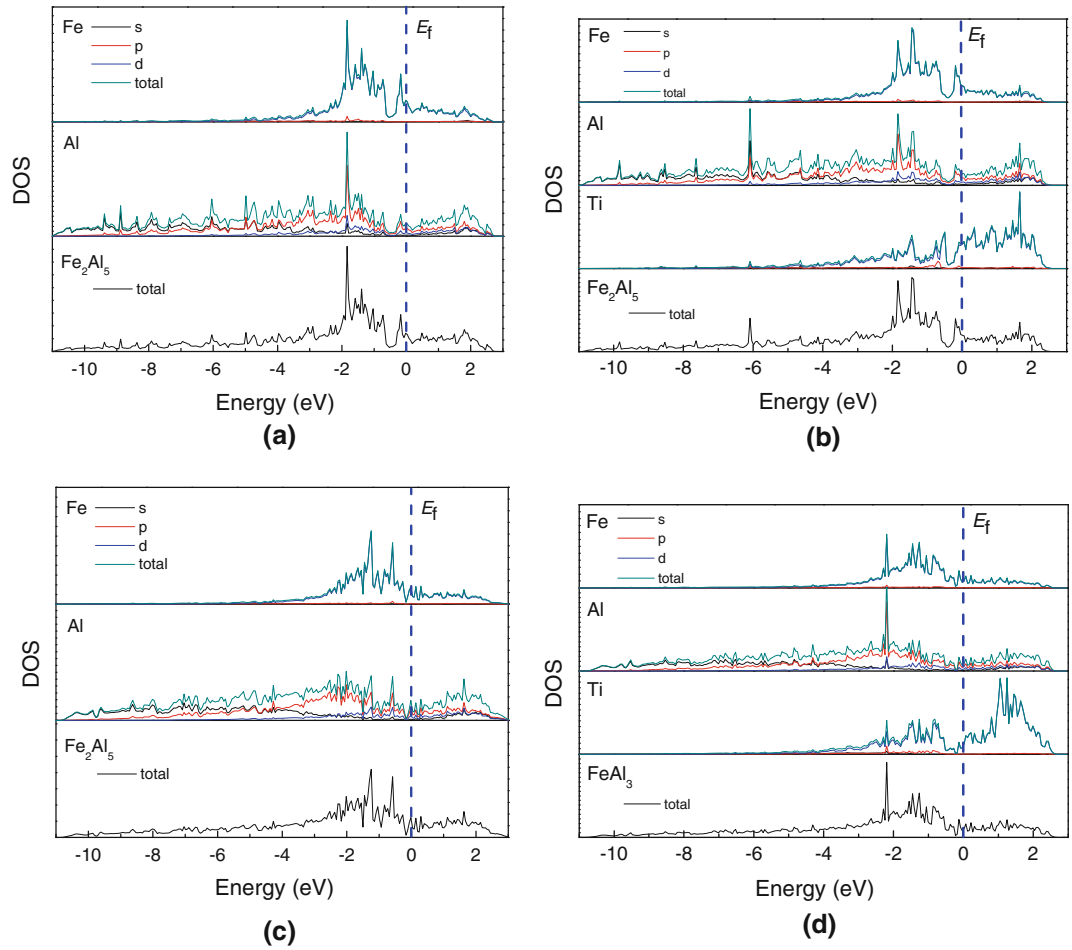

Fig. 3—(*a*) Electronic structure profile of pure, Ti substitution of (*b*) Fe_2Al_5 and (*c*) pure, and (*d*) Ti substitution of $FeAl_3$.

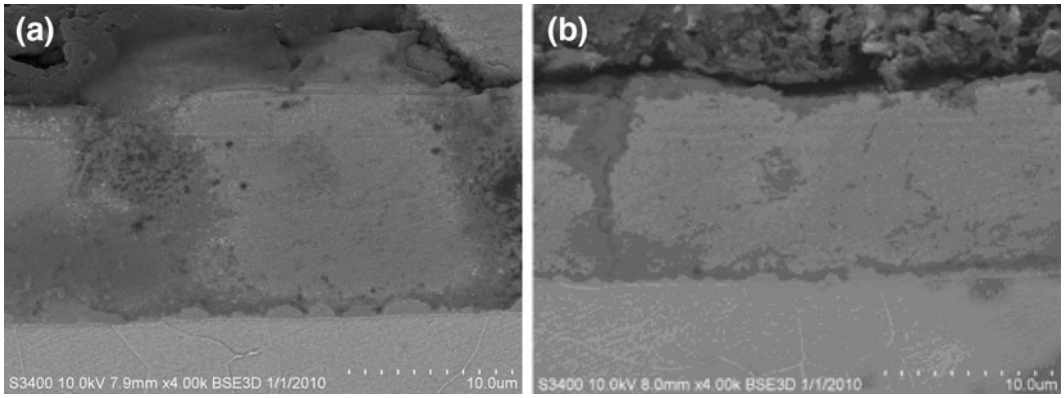

Fig. 4—Cross-sectional observation of the Zn-55Al-1.6Si and Zn-55Al-1.6Si-Ti coating structure.

Bonding energy, charge density, and DOS results show that additional Ti will grab electronic charges from Al atoms and form bonds with neighboring Al, which will prevent the interaction between Fe and Al and reduce the growth of Fe-Al intermetallic layers. Meanwhile, an experiment was performed to validate the prediction results of first-principles successfully.

We deliberately chose to study Ti addition as the dopants' effect on the thickness of the intermetallic layer, because that could influence the adhesion of the coating. In fact, we are now extending our investigations to the interface of the alloy layer/substrate, and we plan to report on these new results in the near future.

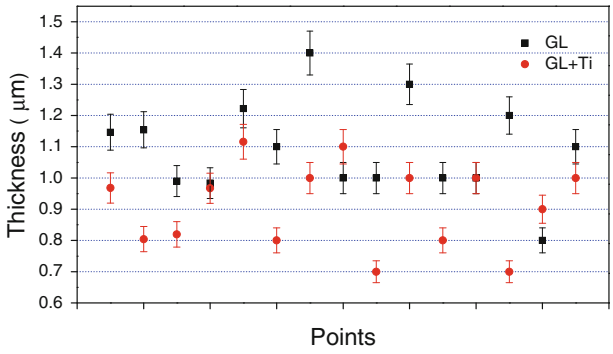

Fig. 5—Effect of Ti addition on the thickness of the intermetallic layer.

ACKNOWLEDGMENTS

The authors thank the National Natural Science Foundation of China (Grant Nos. 51074103 and 51104098) for the financial support and thank Qiang Li and Yuliang Chu, Instrumental Analysis and Research Center, Shanghai University, for their support of the materials testing and research. The computational resources were supported by Associate Professor Yongquan Wu (Shanghai University).

REFERENCES

1. A.R. Marder: *Progr. Mater. Sci.*, 2000, vol. 45, pp. 191–271.
2. N.G. Cho: *Method of Manufacturing a Coated Steel*, Union Steel Manufacturing Co., Ltd., Pusan, KR, 1996.
3. E.T. McDevitt: *Aluminum-Zinc Alloy Composition Comprising Spangle for Hot-Dipping Steel Product, Method and Product Obtainable Thereof*, ISG Technologies Inc., Bethlehem, 2007.
4. B. Xu, D. Phelan, and R. Dippenaar: *Mater. Sci. Eng. A*, 2008, vol. 473, pp. 76–80.
5. K. Honda, K. Ushioda, and W. Yamada: *Cer. Trans.*, 2009, vol. 21, pp. 355–62.
6. B. Xu: Doctoral Degree, University of Wollongong, Wollongong, 2006.
7. F. García, A. Salinas, and E. Nava: *Mater. Lett.*, 2006, vol. 60, pp. 775–78.
8. F. García, A. Salinas-Rodriguez, and E. Nava: *Mater. Sci. Forum*, 2007, vol. 560, pp. 97–102.
9. J.B. Liu: *Hot Dip Aluminumon Steel*, Metallurgy Industry Press, Beijing, 1995 (in Chinese).
10. D. Yang, J. Chen, Q. Han, and K. Liu: *J. Rare Earths*, 2009, vol. 27, pp. 114–18.
11. G. Kresse and J. Furthmuller: *Phys. Rev. B*, 1996, vol. 54, pp. 11169–86.
12. P.E. Blochl: *Phys. Rev. B*, 1994, vol. 50, pp. 17953–79.
13. J.P. Perdew, J.A. Chevary, S.H. Vosko, K.A. Jackson, M.R. Pederson, D.J. Singh, and C. Fiolhais: *Phys. Rev. B*, 1992, vol. 46, p. 6671.
14. M. Methfessel and A.T. Paxton: *Phys. Rev. B*, 1989, vol. 40, pp. 3616–21.
15. D.M. Wood and A. Zunger: *J. Phys. A*, 1985, vol. 18A, pp. 1343–59.
16. W.H. Press, S.A. Teukolsky, and W.T. Vetterling: *Numerical Recipes: The Art of Scientific Computing*, Cambridge University Press, Cambridge, United Kingdom, 1996.
17. L. Stenberg, R. Sjövall, and S. Lidin: *J. Solid State Chem.*, 1996, vol. 124, pp. 65–68.
18. R.W. Richard, R.D. Jones, P.D. Clements, and H. Clarke: *Int. Mater. Rev.*, 1994, vol. 39, pp. 191–212.
19. P. Black: *Acta Crystallogr.*, 1955, vol. 8, pp. 175–82.
20. P. Wu, H.M. Jin, and H.L. Liu: *Chem. Mater.*, 2002, vol. 14, pp. 832–37.
21. H.M. Jin, Y. Li, H.L. Liu, and P. Wu: *Chem. Mater.*, 2000, vol. 12, pp. 1879–83.
22. J.L. Pan, J. Ni, and B. Yang: *Euro. Phys. J. B*, 2010, vol. 73, pp. 367–73.
23. G. Wu, F. Jin, B. Li, J. Chen, J. Zhang, and Q. Li: *2010 4th Baosteel Biennial Academic Conf.*, Shanghai, 2010, pp. D7–D11.
24. G.X. Wu, J.Y. Zhang, Q. Li, and X.C. Wu: *Metall. Mater. Trans. B*, 2012, vol. 43B, pp. 198–205.